Published in final edited form as:
J Mech Behav Biomed Mater. 2011 November ; 4(8): 1627–1636. doi:10.1016/j.jmbbm.2011.03.022.

Fiber Angle and Aspect Ratio Influence the Shear Mechanics of Oriented Electrospun Nanofibrous Scaffolds

Tristan P. Driscoll[1,2], **Nandan L. Nerurkar**[1], **Nathan T. Jacobs**[1,3], **Dawn M. Elliott**[1,2,3], and **Robert L. Mauck**[1,2,3,†]

[1] McKay Orthopaedic Research Laboratory, Department of Orthopaedic Surgery, University of Pennsylvania, Philadelphia, PA 19104

[2] Department of Bioengineering, University of Pennsylvania, Philadelphia, PA 19104

[3] Department of Mechanical Engineering and Applied Mechanics, University of Pennsylvania, Philadelphia, PA 19104

Abstract

Fibrocartilages, including the knee meniscus and the annulus fibrosus (AF) of the intervertebral disc, play critical mechanical roles in load transmission across joints and their function is dependent upon well-defined structural hierarchies, organization, and composition. All, however, are compromised in the pathologic transformations associated with tissue degeneration. Tissue engineering strategies that address these key features, for example, aligned nanofibrous scaffolds seeded with mesenchymal stem cells (MSCs), represent a promising approach for the regeneration of these fibrous structures. While such engineered constructs can replicate native tissue structure and uniaxial tensile properties, the multidirectional loading encountered by these tissues *in vivo* necessitates that they function adequately in other loading modalities as well, including shear. As previous findings have shown that native tissue tensile and shear properties are dependent on fiber angle and sample aspect ratio, respectively, the objective of the present study was to evaluate the effects of a changing fiber angle and sample aspect ratio on the shear properties of aligned electrospun poly(ε-caprolactone) (PCL) scaffolds, and to determine how extracellular matrix deposition by resident MSCs modulates the measured shear response. Results show that fiber orientation and sample aspect ratio significantly influence the response of scaffolds in shear, and that measured shear strains can be predicted by finite element models. Furthermore, acellular PCL scaffolds possessed a relatively high shear modulus, 2–4 fold greater than native tissue, independent of fiber angle and aspect ratio. It was further noted that under testing conditions that engendered significant fiber stretch, the aggregate resistance to shear was higher, indicating a role for fiber stretch in the overall shear response. Finally, with time in culture, the shear modulus of MSC laden constructs increased, suggesting that deposited ECM contributes to the construct shear properties. Collectively, these findings show that aligned electrospun PCL scaffolds are a promising tool for engineering fibrocartilage tissues, and that the shear properties of both acellular and cell-seeded formulations can match or exceed native tissue benchmarks.

†Corresponding Author: Robert L. Mauck, Ph.D., Assistant Professor of Orthopaedic Surgery and Bioengineering, McKay Orthopaedic Research Laboratory, Department of Orthopaedic Surgery, University of Pennsylvania, 36th Street and Hamilton Walk, Philadelphia, PA 19104, Phone: (215) 898-3294, Fax: (215) 573-2133, lemauck@mail.med.upenn.edu.

Keywords

Electrospinning; Mesenchymal Stem Cells; Tissue Engineering; Fibrocartilage; Annulus Fibrosus; Meniscus

Introduction

Fibrocartilages are distributed throughout the body and play critical roles in motion and load transmission across joints. These dense connective tissues are typified by an organized and hierarchically distinct collagenous structure. For example, the knee meniscus, which transmits loads from the femur to the tibia, is composed of highly organized collagen bundles that pass circumferentially through the semi-lunar tissue and provide for its mechanical anisotropy in tension [1–3]. Likewise, the annulus fibrosus (AF) of the intervertebral disc of the spine resists tensile, compressive and shear loading as motion occurs between two adjacent vertebral bodies. The AF is composed of alternating ±30° layers of aligned collagen fibers embedded in a non-fibrillar matrix of hydrated proteoglycans [4, 5]. Proper mechanical function of both the intervertebral disc and the meniscus is dependent upon this structure and composition [6, 7], however, both are compromised in the pathologic transformations associated with tissue degeneration. Current treatments such as meniscectomy (for meniscus) and discectomy and spinal fusion (for AF) aim to relieve pain but are not ideal due to their inability to restore function and their tendency to accelerate degeneration in the joint and/or adjacent discs [8, 9].

Tissue engineering strategies present a promising alternative that could allow for regeneration of these fibrous structures and restoration of native tissue structure and function. Indeed, many groups have explored generation of whole meniscus [10–12], disc analogues [13–15], and disc substructures [16–20] with a variety of materials and starting cell populations. Due to the large and multi-directional forces experienced by these tissues *in vivo*, a successful engineered construct must resist considerable load magnitudes (i.e., multiples of body weight) under tensile, shear, and compressive configurations [21, 22]. For instance, circumferential tensile stresses in the AF (due to pressurization of the nucleus pulposus under axial spinal loads), are often combined with torsional motion of the spine, which generates direct shearing of the AF. The microstructural organization of the native AF is well suited to withstand this loading environment. Accordingly, a structurally motivated tissue engineering strategy may be necessary in order to generate a construct that is functionally commensurate with the native tissue when subject to the full range of loading modalities present *in vivo*.

To specifically address the structural basis of function in engineered tissues, our group and others have employed aligned nanofibrous scaffolds formed by electrospinning [13, 16, 23]. Electrospinning is a scaffold fabrication process in which ultra-fine polymer strands are formed by the electrostatic drawing of a polymer towards a collecting surface [24, 25]. Collection of fibers on a rotating mandrel generates aligned scaffolds [26]. Furthermore, these nanofibrous scaffolds direct meniscus [27], AF [28] and mesenchymal stem cell (MSC) [29] alignment and subsequent matrix deposition, recapitulating tissue micro-architecture [28, 30]. With time in culture after cell seeding, single-lamellar constructs can match mechanical properties of native meniscus [31] and AF [29, 32] when evaluated in tension. These findings suggest that nanofibrous assemblies that mimic the anisotropic and hierarchical structure of the native tissues direct tissue formation and match several key mechanical benchmarks.

While these data suggest promise for this approach to fibrous tissue engineering, the shear properties of such constructs have not yet been evaluated. Thus it is not yet clear whether these nanofiber-based tissue constructs can withstand the considerable shear stresses incurred *in vivo*. Indeed, despite the importance of this loading modality in many tissues, no engineered AF or meniscus construct has been evaluated in shear, and only a small number of studies have quantified the shear properties of the native meniscus and AF [33–37]. Due to the practical difficulty of applying pure shear to a sample, most AF and meniscus shear testing has been performed on cylindrical, cuboidal, or planar samples under compressive or tensile pre-strains. Of these, simple shear of planar samples is appealing because the application of tensile pre-strains allows for combined fiber stretch and shear as it occurs *in situ*. For such a configuration, however, finite element studies of ligament have shown that sample aspect ratio is an important determinant of the strain field, which can be heterogeneous across a sample with magnitudes considerably lower than the applied strain [38]. This is an important consideration for the AF and meniscus, where sample aspect ratio is limited by tissue geometry. Additionally, the effects of fiber orientation and fiber stretch on shear properties is difficult to assess in native tissue [1, 5]. If the shear properties of an engineered meniscus or AF construct are to be deemed adequate, comparisons need to be made to native tissue values.

Thus, the objective of the present study was to quantify the effects of fiber angle and sample aspect ratio on the shear properties of aligned electrospun scaffolds, and to determine how extracellular matrix deposition by resident MSCs modulates the measured shear response. Using experimentally measured scaffold bulk material properties, a finite element model was constructed to determine the effect of aspect ratio and fiber orientation on the shear strain distributions within these nanofibrous assemblies. Next, scaffolds with varying fiber angle were tested in simple shear with two different aspect ratios in order to compare experimentally measured and model predicted strain distributions. Finally, samples with an aspect ratio similar to AF shear testing studies were seeded with MSCs and assayed for functional growth (shear mechanics and biochemistry) with time in culture.

Methods

Scaffold Fabrication

Aligned nanofibrous poly(ε-caprolactone) (PCL) scaffolds were fabricated by electrospinning as described previously [27, 28]. Briefly, a 14.3% w/v solution of PCL (BrightChina, Hong Kong, China) was prepared in a 1:1 mixture of tetrahydrofuran and N, N-dimethylformamide (Fisher Chemical, Fairlawn, NJ). This solution was ejected via syringe pump at 2.5 mL/h through a spinneret charged to +13 kV. Fibers were collected for 6 hours on a grounded rotating mandrel with a surface velocity of 10 m/s. This resulted in a scaffold sheet of ~600 μm thickness from which rectangular samples (3 × 16 mm and 8 × 14 mm) were cut with their long axes oriented at angles of 0°, 30°, 45°, 60° and 90° with respect to the prevailing fiber direction [28]. Samples were stored in a desiccator until mechanical testing or cell seeding.

Shear Mechanical Testing

A custom simple shear testing device was used to measure the shear properties of scaffolds and engineered constructs. Details on device development and validation are provided in [37]. Briefly, the shear device was designed as an attachment to an Instron 5848 (Canton, MA) electromechanical testing system. Samples were placed horizontally between two serrated grips, with one grip attached to the Instron vertical actuator and the other attached to a vertical post mounted on the base-plate of a tank filled with phosphate buffered saline. A horizontal micrometer driven stage was incorporated into the tank to allow for application

of tensile pre-strains in the horizontal direction. A mounting track was employed to align and load samples into the removable grips prior to insertion into the bath. Two load cells were incorporated into the system: a 5 N load cell on the vertical axis to measure shear loads and a 9.8 N submersible load cell (model 31 submersible, Honeywell, Minneapolis, MN) on the horizontal axis to measure tensile loads generated during pre-strain and shearing.

Prior to mechanical testing, sample cross-sectional area was measured using a custom laser device [39]. Samples were then speckle coated with black enamel paint to allow for texture correlation strain analysis (below) [40]. Samples with two different X:Y aspect ratios were investigated (Figure 1). Grip-to-grip distances for 2:1 and 1:2 aspect ratios were 6 mm and 4 mm, respectively. Samples were loaded into the device with fibers oriented oblique to the X-direction by an angle θ, as depicted in Figure 1A. A 1% tensile pre-strain (Figure 1A) was applied along the X-direction and held for 5 minutes. Samples were next preconditioned in shear to ±10° for 20 cycles at 0.05 Hz and then ramped at a rate of 3° per minute to 10° (E_{xy} = ½tan(θ) = 0.088). Images were captured by digital camera (Basler, Exton, PA) every 5 seconds throughout the ramp and used to determine the average Lagrangian shear strain (E_{xy}) for the middle 50% of the sample (Figure 1B) using Vic2D texture correlation software (Correlated Solutions Inc., Columbia, SC). Shear stress was calculated as the measured shear force divided by the cross-sectional area. Apparent shear modulus was calculated from the last 25% of the strain ramp for the stress-strain curve. The deformation gradient tensor was determined from surface deformations and used to calculate fiber stretch, which was defined as the ratio of deformed to undeformed length along the direction of scaffold fiber alignment. Additionally, strain measurements were taken at 10% intervals across the samples using sets of 4 points (Figure 1B) to evaluate strain homogeneity at the peak of the strain ramp.

Modeling

Finite element (FE) modeling was performed in order to predict strain distributions for samples with varying fiber orientations and aspect ratios. This was accomplished using the COMSOL3.5a structural mechanics module (COMSOL, Burlington, MA) with an assumption of plane stress. The scaffold was taken to be linearly elastic and transversely isotropic, which required five independent mechanical properties (E_x = 28 MPa, E_y = 3 MPa, v_{xy} = 0.4, v_{yz} = 0.2 and G_{xy} = 1.6 MPa). These values were determined experimentally [41]. The material axis was defined using a second material coordinate system that was rotated by the angle θ = 30°, 60° or 90° about the z-axis so that each experimentally tested fiber orientation could be captured via the same five input parameters. Shear was applied with a prescribed displacement boundary condition in the global coordinate system. Solutions were visualized as contour plots of the shear strain (E_{xy}) and strains along the centerline were used for comparison with experimental results.

Cell-Seeded Construct Culture and Analysis

Cell-laden constructs were formed by seeding electrospun scaffolds with MSCs and culturing under pro-fibrochondrogenic conditions for up to 12 weeks [27, 31]. MSCs were isolated from the femurs and tibiae of two 3–6 month old calves within 12 hours of slaughter, as described previously [42, 43]. Cells were expanded on tissue culture plastic in basal medium (high glucose DMEM containing 1% penicillin, streptomycin, fungizone and 10% fetal bovine serum) to passage 2. Scaffolds with fiber orientations of 0°, 45° and 60° were sterilized and rehydrated using decreasing concentrations of ethanol (100, 70, 50, 30%, 1 hr/step) and then washed for 1 hour in PBS. Scaffolds were then incubated in 20 μg/mL fibronectin in PBS for 16 hours and washed again with PBS prior to seeding [29]. Scaffolds were seeded and cultured in non-tissue culture treated six-well plates. Each scaffold received 50 μL of cell solution (1×10^7 cells/mL) on one side followed by a one hour incubation at

37 °C. The opposite side of each scaffold was then seeded with another 50 μL of cell solution and incubated for an additional two hours. Each well was then filled with 4 mL of basal media, which was replaced after 24 hours with 4 mL of a chemically defined media (DMEM, 0.1 mM dexamethasone, 40 mg/mL L-Proline, 100 mg/mL Sodium Pyruvate, 1% Insulin, Transferrin, Selenium/Premix, and 1% penicillin, streptomycin and fungizone supplemented with 10 ng/mL Transforming Growth Factor-β3). Chemically defined media was replaced twice weekly for the duration of the study.

At 4, 8 and 12 weeks, samples were removed from culture and subjected to simple shear testing (as above) followed by biochemical analyses (n = 5/orientation/time point). Following mechanical testing, dry weight was measured following 24 hours lyophilization, and samples digested with papain [27]. Total collagen, glycosaminoglycan and DNA content were determined using the ortho-hydroxyproline assay (OHP), 1,9-dimethylmethylene blue (DMMB) dye binding assay and the PicoGreen assay, respectively, and each were normalized to the sample dry weight [31, 44]. Additional samples (n=2/group/timepoint) were used for histological staining of collagens and glycosaminoglycans using picrosirius red and alcian blue, respectively.

Statistics

The effect of fiber orientation on shear modulus was evaluated by one-way analysis of variance with Tukey's *post hoc* test, with significance set at $P < 0.05$. Comparisons of shear modulus were made between fiber orientations for a given aspect ratio. Additionally, comparisons of shear modulus for cell-seeded constructs were made between time-points. Pearson's comparison was performed for linear correlation between fiber stretch and shear modulus with goodness of fit represented as R^2 values and significance for deviation from zero set at $P < 0.05$. Samples with fiber stretch less than 1.0 (fiber compression and buckling) were not included in the linear correlations.

Results

Influence of Fiber Angle and Sample Aspect Ratio on Strain Homogeneity

Based on previous theoretical models [38] and anatomic constraints on native tissue sample geometry, two different aspect ratios were evaluated, 1:2 or 2:1 with respect to the gauge length. Finite element analysis showed that samples with a 1:2 aspect ratio had a more homogeneous distribution of shear strain for each fiber orientation (Figure 2). Moreover, predicted peak shear strain values for the 1:2 condition were very close to the 0.088 applied shear strain (Figure 2). In addition to their dependence on aspect ratio, predicted shear strain magnitudes and distributions were dependent on the fiber orientation of the scaffold. This variation was most noticeable for the 2:1 aspect ratio, where the peak strain decreased as the fiber angle increased. For the 2:1 aspect ratio, the 0° model attained strain in central regions of ~0.08 (compared to the 0.088 shear strain applied to the boundaries), while for samples with fiber directions of 60° and 90°, central strain decreased to ~0.04 (Figure 3A). Modeling of the 1:2 aspect ratio showed less variation in the magnitude of strain in the central region, with all orientations displaying strain magnitudes close to the 0.088 applied strain (Figure 3C).

When these two configurations were evaluated experimentally through surface analysis, measured strains were similar to those predicted by the FE model (Figure 3). Overall, the observed strains for the 1:2 aspect ratio were larger and more homogeneous than those observed for the 2:1 aspect ratio and while the 60° samples show some inhomogeneity at the edges, central region strains were relatively homogeneous and very close to the 0.088 applied strain. The experimentally measured shear strain was normalized to the applied

shear strain and plotted as a function of marker location (Figures 3B and 3D). For the 2:1 aspect ratio, the magnitude of the measured strains decreased considerably as the fiber angle increased, and the 60° and 90° samples had very low strains across the entire scaffold expanse (Figure 3B). The FE model successfully predicted this inhomogeneous strain distribution as well as the changing strain magnitudes as fiber angle increased for 2:1 samples (Figure 3A). For the 1:2 aspect ratio, strains at the top and bottom edges of the samples were low and the strains became less homogeneous as the fiber angle increased (Figure 3D). The magnitude and distribution of these experimentally measured strains also corresponded well with the model-predicted strains for this 1:2 aspect ratio (Figure 3C).

Influence of Fiber Angle and Aspect Ratio on Measured Shear Properties

The shear modulus was next computed from mechanical tests, using the average shear strain in the middle 50% of each sample. This is an average strain for the entire region bounded by the red points shown in Figure 1B. The apparent shear modulus of scaffolds was dependent on the sample aspect ratio. For the 2:1 aspect ratio, fiber orientation had an effect on the apparent shear modulus only for the 30° samples compared to 0° and 60° ($P < 0.05$; Figure 4A). In contrast, for the 1:2 aspect ratio, the apparent shear modulus of the 30°, 45° and 60° samples were all significantly higher than the other fiber orientations ($P < 0.05$; Figure 4B).

Observed fiber stretch corresponded well with the apparent shear modulus. The 2:1 samples had a significantly higher fiber stretch ($P < 0.05$) for the 30° orientation, and likewise had a higher apparent shear modulus (Figure 5A). However, because little fiber stretch was observed in all other fiber orientations for this aspect ratio, the correlation of fiber stretch with the apparent shear modulus was not significant and the slope was not different from zero ($R^2 = 0.22$, slope = 30.3 ± 15.1, $P = 0.064$, Figure 5B). Conversely, the 1:2 aspect ratio samples had higher fiber stretch ratios, which were dependent on fiber orientation (Figure 5C). Moreover, there was good correlation between fiber stretch and apparent shear modulus ($R^2 = 0.51$, Figure 5D), with a slope that deviated significantly from zero (slope = 83.6 ± 19.9, $P < 0.001$).

Influence of Extracellular Matrix Deposition on Shear Properties in MSC Seeded Constructs

The 2:1 aspect ratio was chosen for cell seeded experiments so that comparisons could be made with native AF and meniscus tissues, where sample size is limited by anatomical shape. Samples with $\theta = 0°$, 45° and 60° fiber orientations were chosen due to their relevance to the physiologic shearing of the meniscus and intervertebral disc that occurs with load bearing. From 0 to 12 weeks, the apparent shear modulus for $\theta = 45°$ samples increased by ~30% ($P < 0.05$; Figure 6A). Increases for $\theta = 0°$ and 60° constructs trended upwards ($P < 0.12$). DNA, s-GAG, and collagen content did not significantly vary between fiber orientations, and so data was pooled for 0°, 45° and 60° samples. DNA content per dry weight decreased significantly from week 4 to weeks 8 and 12 ($P < 0.05$, Figure 6B), while s-GAG (Figure 6C) and collagen (Figure 6D) content increased significantly over this same time course ($P < 0.05$). Deposition of GAG and collagen was observed throughout the scaffold thickness (Figure 6E).

Discussion

Dense fibrocartilaginous tissues such as the knee meniscus and the AF of the intervertebral disc present considerable challenges for tissue engineering and regenerative medicine. The low cellularity and vascularity of these tissues in the adult limits intrinsic repair, while the ordered structure defines precise mechanical functionalities that are difficult to reproduce in synthetic implants. Oriented electrospun nanofibrous scaffolds prescribe cell, and

subsequently, matrix directionality. These biomaterials recreate several key attributes of fiber-reinforced tissues, including mechanical anisotropy in tension. When seeded with cells, these constructs mature *in vitro* and match key mechanical benchmarks, including a near-native uniaxial tensile modulus [25]. However, fibrocartilages are exposed to dynamic and multi-directional loads (including compression and shear) *in vivo*, and successful implementation of an engineered replacement tissue will likely also require mechanical functionality in this context. To address this, the present study evaluated the properties of aligned nanofibrous electrospun scaffolds with varying aspect ratios and fiber orientations in simple shear. Fiber orientation was analyzed given its physiologic relevance and direct correlation with tensile properties [28], while aspect ratios were considered given past findings of shear strain inhomogeneity in oriented tissues such as tendon and ligament [38]. Alterations in shear properties were also evaluated as a function of matrix deposition for mesenchymal stem cell seeded constructs. Fiber orientation and sample aspect ratio significantly influenced the response of scaffolds in shear and, with time in culture, the shear modulus of MSC laden constructs increased.

In addition to their potential for directing tissue formation for replacement of degenerate disc and meniscus, nanofibrous scaffolds also serve as useful analogs for understanding structure-function relationships in fiber-reinforced materials, and in constructs as they change with matrix deposition [45] or with or material degradation [46]. Within both acellular and cell-seeded scaffolds, one can readily alter a number of structural parameters, including the degree of fiber dispersion [26], the connectivity between fibers [47], and fiber orientation with respect to testing direction [28]. These parameters are difficult or impossible to precisely control using native tissue samples, given constraints of samples size, matrix organization, and composition.

In addition to control of structural parameters, relatively simple linear and transversely isotropic finite element models can be used to describe deformation of these nanofibrous scaffolds under varying boundary conditions and sample sizes with good fidelity. For example, in this study, measured and predicted shear strain distributions in oriented scaffolds corresponded very well with one another. This is further confirmed by the finding of a maximum shear strain in samples of ~50% of applied shear for 90° samples, consistent with [38]. These findings indicate, as shown previously for uniaxial tension [32], that shear deformations of these scaffolds can be modeled using continuum assumptions.

Having validated the shear testing methods for this study, we next determined the shear modulus of oriented scaffolds across a range of fiber angles and aspect ratios. For these studies, shear strain was captured in the inner 50% of the scaffold width (Figure 1B), where strains were most homogenous, regardless of aspect ratio. Results demonstrated that both aspect ratio and fiber orientation influence the apparent shear modulus. For samples with a 2:1 aspect ratio, only one orientation (30°) resulted in an increased apparent shear modulus relative to other orientations. Conversely, for the 1:2 aspect ratio, apparent shear modulus of samples with orientations of 30°, 45°, and 60° were higher than 0° or 90°. Computation of fiber stretch from surface strain measurements helps to explain these findings: i.e., when minimal fiber stretch occurs, little direction-dependence is observed in the apparent shear modulus, while when fiber stretch is maximized, apparent shear modulus increases. For example, the 2:1 samples showed increased fiber stretch only for the 30° samples, which had a higher apparent shear modulus. In the 1:2 aspect ratio samples, where fiber stretch was high for all off-axis orientations, correspondingly higher apparent shear moduli were measured.

Given the translational potential of these scaffolds for meniscus and AF repair, it is also useful to compare their measured properties to those reported for native tissue. Native

annulus fibrosus has a shear modulus of 200 – 500 kPa [35, 37]. These values are for AF samples with multiple lamellae oriented at ±30° with respect to the shearing direction. This would correspond to 60° samples tested in this study, which had an apparent shear modulus of ~2,500 kPa as acellular scaffolds, and increased to ~4,000 kPa with time in culture as single-layer MSC-seeded constructs. The addition of a second layer with −60° fiber orientation would most likely decrease the apparent shear modulus as it would increase the cross sectional area but provide a layer undergoing no fiber stretch. Like the AF, the meniscus shear modulus ranges from 100 – 400 kPa [33, 34]. Shearing in the meniscus would correspond to the 0° samples tested in this study, whose shear moduli were ~2,500 kPa, both as acellular scaffolds and with time in culture. Reported values for both AF and meniscus shear properties from the literature are for testing configurations in which minimal fiber stretch occurs, and so primarily represent the extrafibrillar 'matrix' shear properties [48].

Even in the absence of fiber stretch, the measured shear modulus of electrospun scaffolds was quite high (~2MPa). This apparent shear modulus can be thought of as an extrafibrillar 'matrix' shear modulus, which, in the case of acellular scaffolds, reflects the connectivity of fibers to one another as well as the frictional interactions that resist reorientation with shear deformation. When fiber stretch does occur, the apparent shear modulus is additive of this baseline matrix shear modulus and contributions from fiber stretch. This 'matrix' shear modulus for the nanofibrous constructs in this study is up to one order of magnitude higher than native values, even for unseeded scaffolds. A defining challenge of fibrocartilage tissue engineering arises from the natural design of these tissues, which enables resistance to very large stresses in tension while permitting large deformations under shear stresses. From a design/tissue engineering perspective, this is a significant challenge that must be addressed through scaffold modifications and directed tissue deposition. For example, the cell generated extracellular matrix is likely more deformable in shear than the PCL scaffold, and so a more rapidly degrading polymer, such as poly(lactic-co-glycolic acid) [46], may bring shear properties closer to native values as it degrades and is replaced by cell generated extracellular matrix.

There are a number of additional considerations that these findings motivate. First, this study only addressed the quasi-static response of scaffolds and constructs in shear, whereas physiologic loading is generally dynamic. Additionally, the use of structures reinforced by a single fiber population makes comparisons to native tissue difficult: both the AF (+/− 30°) and the meniscus (0°/90°) are multi-lamellar structures. Future studies will thus investigate shear properties of nanofibrous laminates for a range of ply angles, under both quasi-static and dynamic testing modalities. This will not only improve comparisons to native tissues, but will allow for analysis of inter-lamellar connections in shear, which contribute to uniaxial tensile properties through an inter-lamellar shearing mechanism [29]. These assemblies may also allow for better interpretation of native tissue shear testing results, where tested samples are less controlled, more heterogeneous, and have more variable fiber orientation and lamellar proportions. Another limitation of this study is that the measure of fiber stretch used is an approximation based on continuum assumptions. While these assumptions seem valid for shear, future studies will aim to verify that fibers obey this affine prediction. Future studies will also investigate the use of scaffolds with multiple polymer components. These fibrous composite scaffolds allow for manipulation of scaffold mechanical and structural parameters [46, 49]. For instance, by including a population of sacrificial poly(ethylene oxide) fibers, scaffold pore sizes can be increased to promote cellular infiltration [49]. Likewise, manipulation of solvent volatility can be used to modulate fiber-fiber connectivity [47] and its role in establishing the 'matrix' shear modulus in these constructs can be assessed. Indeed, these two last features may be used to 'design

down' the shear properties of scaffolds to better match native tissue levels and so avoid aberrantly high shear stresses immediately upon implantation.

Conclusions

If engineered fibrocartilage constructs are to be successful, they must function adequately in the multidirectional loading environment they will be subjected to when implanted *in vivo*. This will require that they resist tensile, compressive and shear loading. Proper analysis of these constructs in shear requires a thorough understanding of the testing method, which, in the case of simple shear testing, is dependent upon the fiber orientation and aspect ratio of the sample. For aligned electrospun scaffolds, a 2:1 aspect ratio results in low fiber stretch and minimal dependence on fiber orientation, while a 1:2 aspect ratio increases fiber stretch so that mechanical anisotropy in shear is observed. Additionally, MSC generated matrix enhances the properties of these constructs in shear. While the shear properties of these constructs appear to be more than adequate, it is likely that additional processing techniques will be necessary to obtain shear properties closer to native values.

Acknowledgments

This work was supported with funding from the National Institutes of Health (R01 EB02425, R01 AR056624, and T32 AR007132) and the Penn Center for Musculoskeletal Disorders. The authors gratefully acknowledge Dr. Jeffrey Weiss (University of Utah) for provision of shear testing device design.

References

1. Petersen W, Tillmann B. Collagenous fibril texture of the human knee joint menisci. Anat Embryol (Berl). 1998; 197(4):317–24. [PubMed: 9565324]
2. Setton LA, et al. Biomechanical factors in tissue engineered meniscal repair. Clin Orthop. 1999; (367 Suppl):S254–72. [PubMed: 10546651]
3. Proctor CS, et al. Material properties of the normal medial bovine meniscus. J Orthop Res. 1989; 7(6):771–82. [PubMed: 2677284]
4. Hickey DS, Hukins DW. X-ray diffraction studies of the arrangement of collagenous fibres in human fetal intervertebral disc. J Anat. 1980; 131(Pt 1):81–90. [PubMed: 7440405]
5. Cassidy JJ, Hiltner A, Baer E. Hierarchical structure of the intervertebral disc. Connective Tissue Research. 1989; 23:75–88. [PubMed: 2632144]
6. Fithian DC, Kelly MA, Mow VC. Material properties and structure-function relationships in the menisci. Clin Orthop. 1990; (252):19–31. [PubMed: 2406069]
7. Humzah MD, Soames RW. Human intervertebral disc: structure and function. Anat Rec. 1988; 220(4):337–56. [PubMed: 3289416]
8. Harrop JS, et al. Lumbar adjacent segment degeneration and disease after arthrodesis and total disc arthroplasty. Spine. 2008; 33(15):1701–7. [PubMed: 18594464]
9. Levin DA, Hale JJ, Bendo JA. Adjacent segment degeneration following spinal fusion for degenerative disc disease. Bull NYU Hosp Jt Dis. 2007; 65(1):29–36. [PubMed: 17539759]
10. Ballyns JJ, et al. Image-guided tissue engineering of anatomically shaped implants via MRI and micro-CT using injection molding. Tissue Eng Part A. 2008; 14(7):1195–202. [PubMed: 18593357]
11. Chiari C, et al. A tissue engineering approach to meniscus regeneration in a sheep model. Osteoarthritis Cartilage. 2006; 14(10):1056–65. [PubMed: 16731009]
12. Kelly BT, et al. Hydrogel meniscal replacement in the sheep knee: preliminary evaluation of chondroprotective effects. Am J Sports Med. 2007; 35(1):43–52. [PubMed: 16957008]
13. Nesti LJ, et al. Intervertebral disc tissue engineering using a novel hyaluronic acid-nanofibrous scaffold (HANFS) amalgam. Tissue Eng Part A. 2008; 14(9):1527–37. [PubMed: 18707229]
14. Mizuno H, et al. Biomechanical and biochemical characterization of composite tissue-engineered intervertebral discs. Biomaterials. 2006; 27(3):362–70. [PubMed: 16165204]

15. Nerurkar NL, et al. Engineered disc-like angle-ply structures for intervertebral disc replacement. Spine (Phila Pa 1976). 2010; 35(8):867–73. [PubMed: 20354467]
16. Gruber HE, et al. Culture of human anulus fibrosus cells on polyamide nanofibers: extracellular matrix production. Spine. 2009; 34(1):4–9. [PubMed: 19127155]
17. Sato M, et al. Tissue engineering of the intervertebral disc with cultured annulus fibrosus cells using atelocollagen honeycomb-shaped scaffold with a membrane seal (ACHMS scaffold). Medical & Biological Engineering & Computing. 2003; 41(3):365–371. [PubMed: 12803304]
18. Wilda H, Gough JE. In vitro studies of annulus fibrosus disc cell attachment, differentiation and matrix production on PDLLA/45S5 Bioglass composite films. Biomaterials. 2006; 27(30):5220–9. [PubMed: 16814857]
19. Baer AE, et al. Collagen gene expression and mechanical properties of intervertebral disc cell-alginate cultures. J Orthop Res. 2001; 19(1):2–10. [PubMed: 11332616]
20. Chou AI, Akintoye SO, Nicoll SB. Photo-crosslinked alginate hydrogels support enhanced matrix accumulation by nucleus pulposus cells in vivo. Osteoarthritis Cartilage. 2009
21. Nerurkar NL, Elliott DM, Mauck RL. Mechanical design criteria for intervertebral disc tissue engineering. J Biomech. 2010; 43(6):1017–30. [PubMed: 20080239]
22. Vadher SP, et al. Finite element modeling following partial meniscectomy: effect of various size of resection. Conf Proc IEEE Eng Med Biol Soc. 2006; 1:2098–101. [PubMed: 17946937]
23. Yang L, et al. Polar surface chemistry of nanofibrous polyurethane scaffold affects annulus fibrosus cell attachment and early matrix accumulation. J Biomed Mater Res A. 2008
24. Li WJ, et al. A three-dimensional nanofibrous scaffold for cartilage tissue engineering using human mesenchymal stem cells. Biomaterials. 2005; 26(6):599–609. [PubMed: 15282138]
25. Mauck RL, et al. Engineering on the Straight and Narrow: The Mechanics of Nanofibrous Assemblies for Fiber-Reinforced Tissue Regeneration. Tissue Eng Part B Rev. 2009; 15(2):171–193. [PubMed: 19207040]
26. Li WJ, et al. Engineering controllable anisotropy in electrospun biodegradable nanofibrous scaffolds for musculoskeletal tissue engineering. J Biomech. 2007; 40(8):1686–93. [PubMed: 17056048]
27. Baker BM, Mauck RL. The effect of nanofiber alignment on the maturation of engineered meniscus constructs. Biomaterials. 2007; 28(11):1967–77. [PubMed: 17250888]
28. Nerurkar NL, Elliott DM, Mauck RL. Mechanics of oriented electrospun nanofibrous scaffolds for annulus fibrosus tissue engineering. J Orthop Res. 2007; 25(8):1018–28. [PubMed: 17457824]
29. Nerurkar NL, et al. Nanofibrous biologic laminates replicate the form and function of the annulus fibrosus. Nat Mater. 2009; 8(12):986–92. [PubMed: 19855383]
30. Nerurkar, N., et al. Engineering of fiber-reinforced tissue with anisotropic biodegradable nanofibrous scaffolds; Transactions of IEEE Engineering in Medicine and Biology Society; 2006.
31. Baker BM, et al. The influence of an aligned nanofibrous topography on human mesenchymal stem cell fibrochondrogenesis. Biomaterials. 3124:6190–200.
32. Nerurkar NL, Mauck RL, Elliott DM. ISSLS prize winner: Integrating theoretical and experimental methods for functional tissue engineering of the annulus fibrosus. Spine (Phila Pa 1976). 2008; 33(25):2691–701. [PubMed: 19018251]
33. Anderson DR, et al. Viscoelastic shear properties of the equine medial meniscus. J Orthop Res. 1991; 9(4):550–8. [PubMed: 2045982]
34. Zhu W, Chern KY, Mow VC. Anisotropic viscoelastic shear properties of bovine meniscus. Clin Orthop. 1994; (306):34–45. [PubMed: 8070209]
35. Fujita Y, et al. Anisotropic shear behavior of the annulus fibrosus: effect of harvest site and tissue prestrain. Med Eng Phys. 2000; 22(5):349–57. [PubMed: 11121768]
36. Iatridis JC, et al. Shear mechanical properties of human lumbar annulus fibrosus. J Orthop Res. 1999; 17(5):732–7. [PubMed: 10569484]
37. Jacobs NT, et al. Effect of Orientation and Targeted Extracellular Matrix Degradation on Annulus Fibrosus Shear Mechanical Properties. JMBBM. In Review.
38. Gardiner JC, Weiss JA. Simple shear testing of parallel-fibered planar soft tissues. J Biomech Eng. 2001; 123(2):170–5. [PubMed: 11340878]

39. Peltz CD, et al. Mechanical properties of the long-head of the biceps tendon are altered in the presence of rotator cuff tears in a rat model. J Orthop Res. 2009; 27(3):416–20. [PubMed: 18924143]
40. Nerurkar NL, et al. Homologous structure-function relationships between native fibrocartilage and tissue engineered from MSC-seeded nanofibrous scaffolds. Biomaterials.
41. Heo, SC., et al. Microstructure dictates stretch-induced cell and nucleus reorganization on aligned nanofibrous scaffolds. Transactions of the 56th Annual Meeting of the Orthopaedic Research Society; 2011.
42. Huang AH, et al. Tensile properties of engineered cartilage formed from chondrocyte- and MSC-laden hydrogels. Osteoarthritis Cartilage. 2008; 16(9):1074–82. [PubMed: 18353693]
43. Mauck RL, Yuan X, Tuan RS. Chondrogenic differentiation and functional maturation of bovine mesenchymal stem cells in long-term agarose culture. Osteoarthritis Cartilage. 2006; 14(2):179–89. [PubMed: 16257243]
44. Huang AH, Stein A, Mauck RL. Evaluation of the complex transcriptional topography of mesenchymal stem cell chondrogenesis for cartilage tissue engineering. Tissue Eng Part A 16(9). : 2699–708.
45. Nerurkar, NL., et al. Selective removal of extracellular matrix components reveals homologous structure-function relationships between engineered and native fibrocartilage. Transactions of the 56rd Annual Meeting of the Orthopaedic Research Society; New Orleans, LA. 2010.
46. Baker BM, et al. Fabrication and modeling of dynamic multipolymer nanofibrous scaffolds. J Biomech Eng. 2009; 131(10):101012. [PubMed: 19831482]
47. Kidoaki S I, Kwon K, Matsuda T. Mesoscopic spatial designs of nano- and microfiber meshes for tissue-engineering matrix and scaffold based on newly devised multilayering and mixing electrospinning techniques. Biomaterials. 2005; 26(1):37–46. [PubMed: 15193879]
48. Yin L, Elliott DM. A homogenization model of the annulus fibrosus. J Biomech. 2005; 38(8): 1674–84. [PubMed: 15958225]
49. Baker BM, et al. The potential to improve cell infiltration in composite fiber-aligned electrospun scaffolds by the selective removal of sacrificial fibers. Biomaterials. 2008; 29(15):2348–58. [PubMed: 18313138]

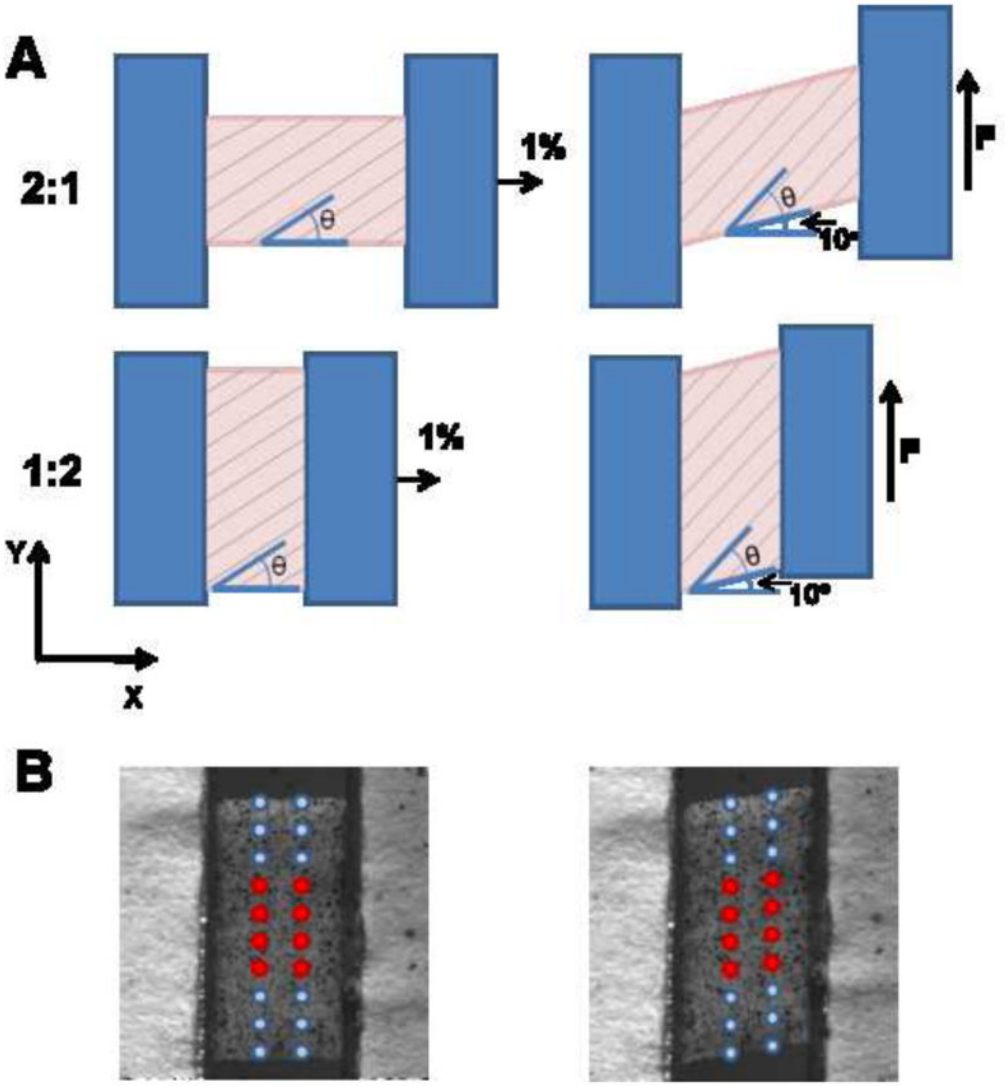

Figure 1.

Schematic representation (**A**) for coordinate system, pre-strain (1%) and shear loading with force F to 10° for samples with aspect ratios of 2:1 and 1:2 and with changing fiber angle θ. Strain marker positioning (**B**) shown on speckle-coated 1:2 sample for modulus calculation (red) and strain homogeneity analysis (red and blue).

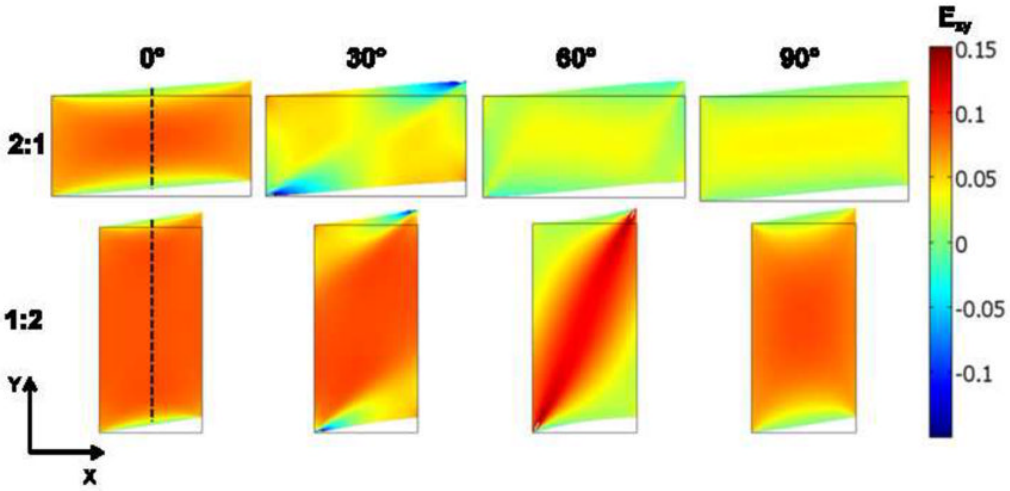

Figure 2.

Finite element analysis of planar samples in simple shear with different aspect ratios (2:1 and 1:2) as a function of varying fiber orientation (0°, 30°, 60°, 90°). Surface plots depict Lagrangian shear strain (E_{xy}). Dotted line indicates the centerline used for comparison to experimental results.

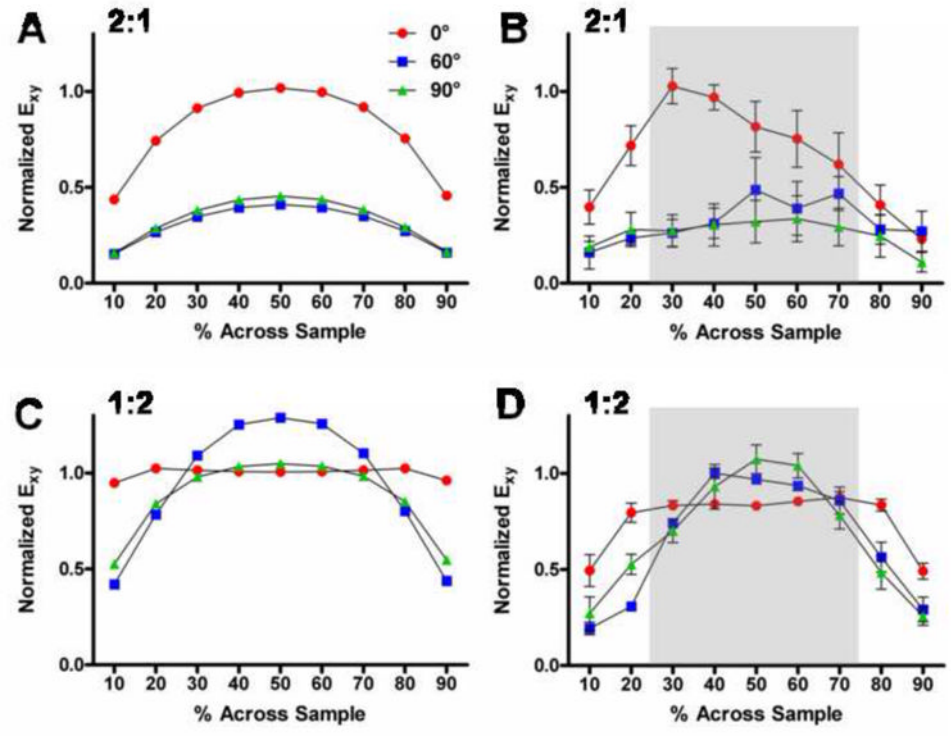

Figure 3.

Model predicted (**A,C**) and experimentally measured (**B,D**) strain distribution across electrospun scaffolds in the Y direction along the centerline for samples with a 2:1 (**A,B**) and 1:2 (**C,D**) aspect ratio. Grey region indicates the relatively homogeneous strain region that was used for calculation of shear modulus. Strain is normalized to the applied strain (E_{xy} = 0.088). Experimental results indicate mean ± SEM (n=5 per θ).

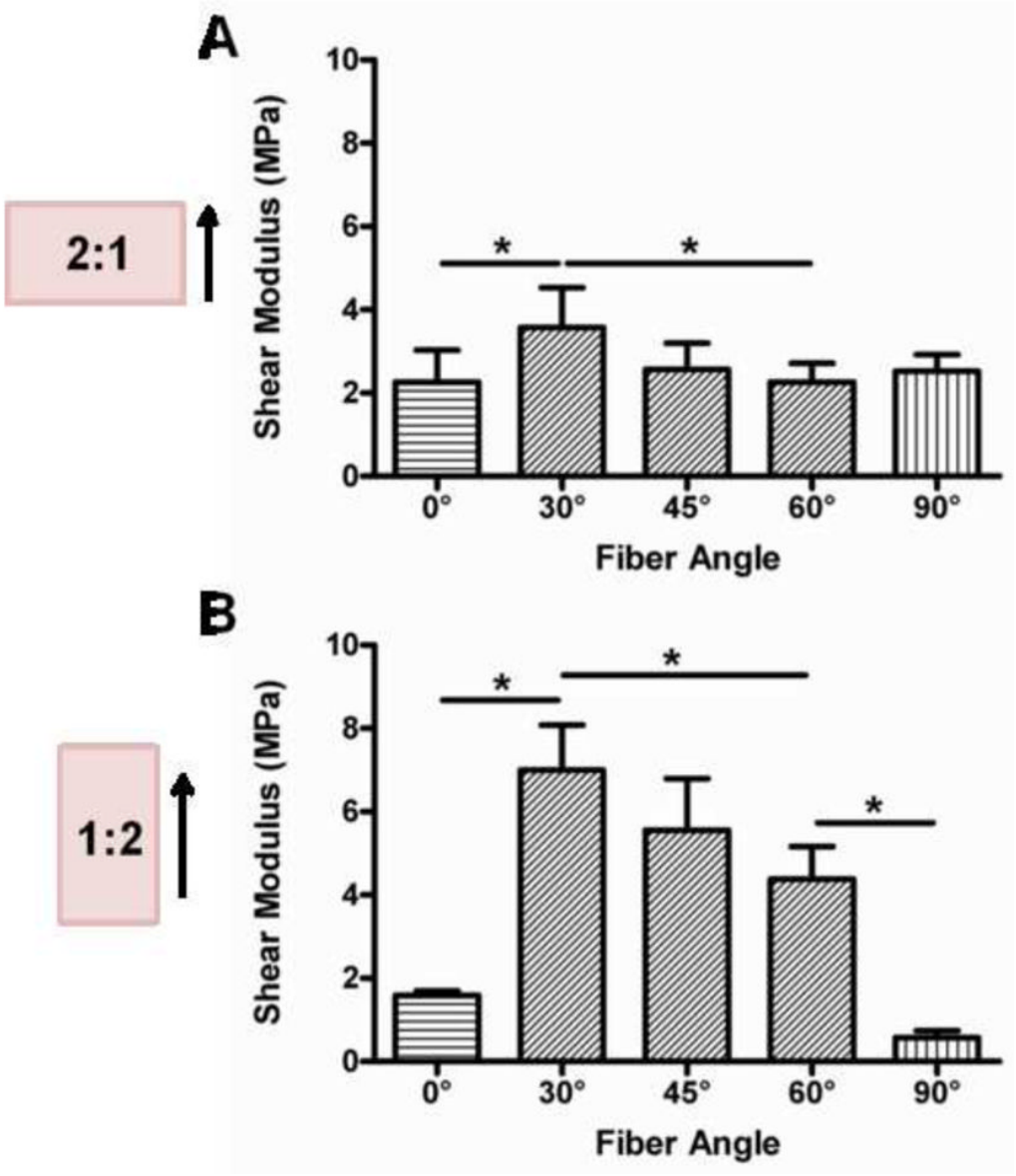

Figure 4.

Experimentally measured apparent shear moduli for samples with a 2:1 (**A**) or 1:2 (**B**) aspect ratio. * = $P < 0.05$ between indicated fiber angles. Results indicate mean ± SD (n = 5 per θ).

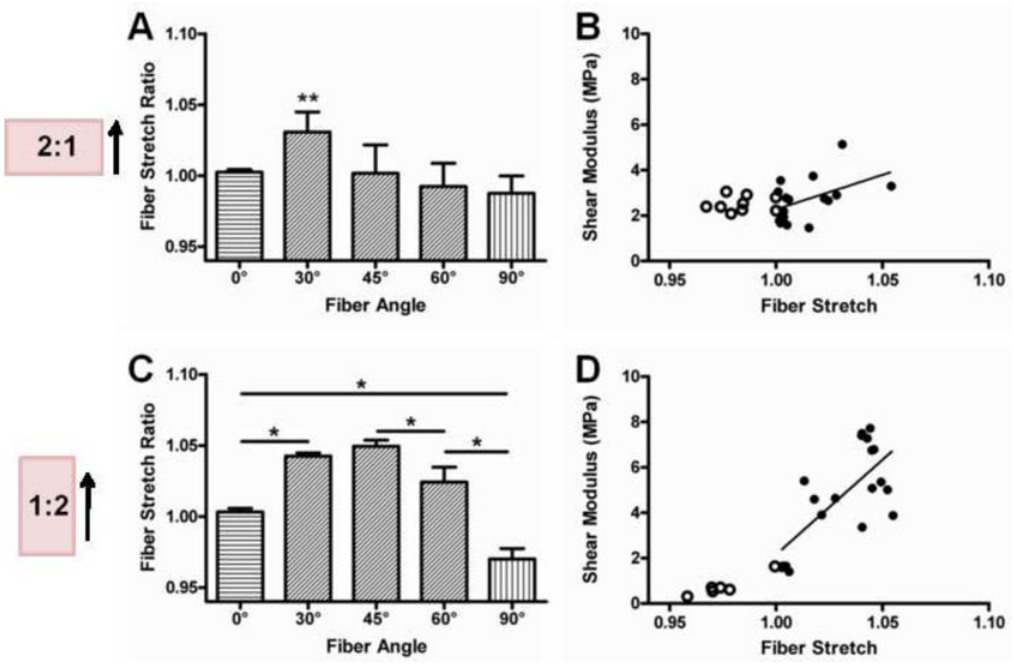

Figure 5.

Experimentally measured fiber stretch ratios (**A,C**) for samples with a 2:1 (**A–B**) or 1:2 (**C–D**) aspect ratio with correlation plots of shear modulus vs. fiber stretch (**B,D**). Open circles indicate samples with fiber stretch less than 1 which were not included in the regression analysis. * = $P < 0.05$ between indicated fiber angles, ** = $P < 0.05$ compared to 0°, 60° and 90°. Results indicate mean ± SD (n = 5 per θ).

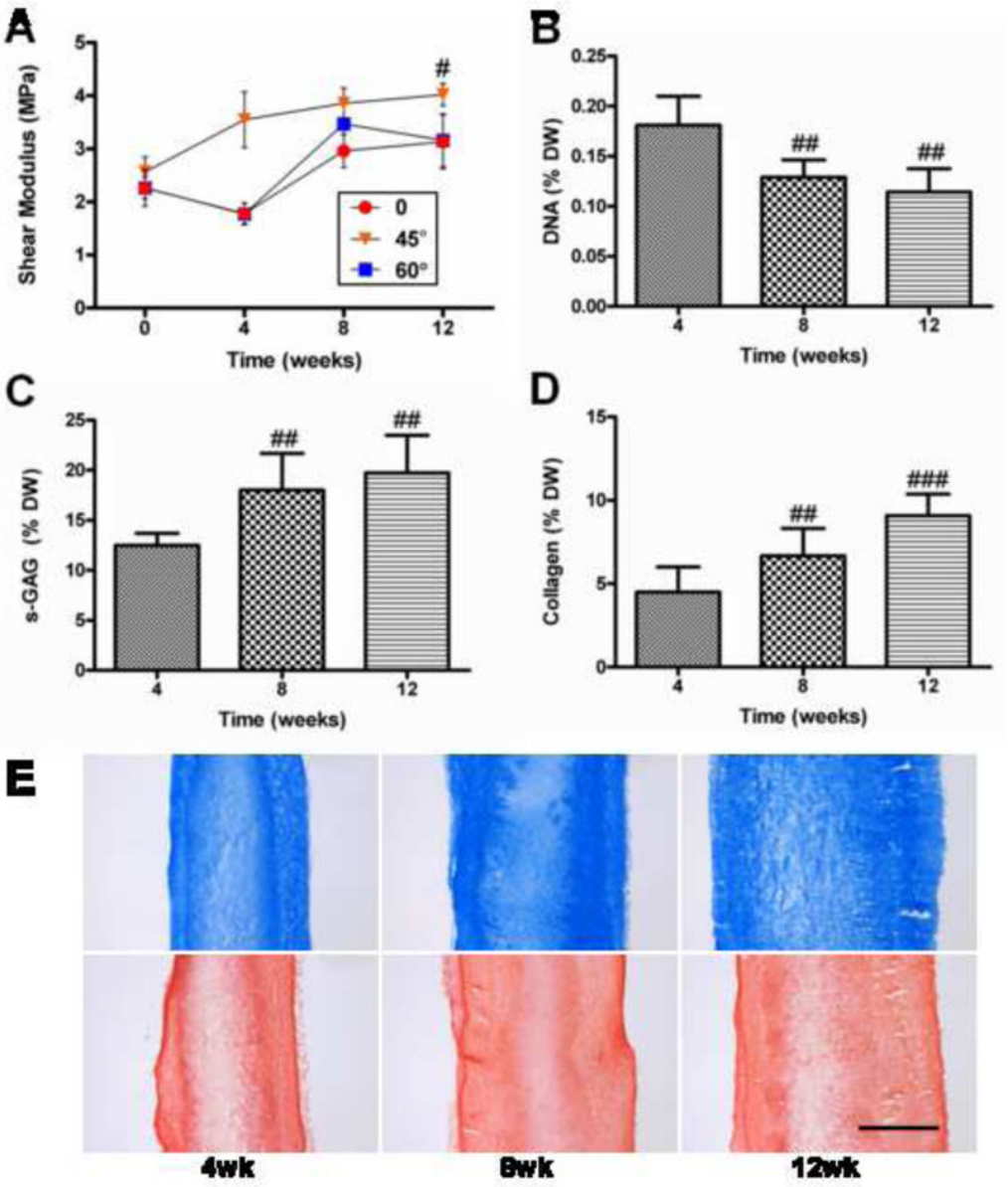

Figure 6.

Functional growth of MSC-laden constructs with fiber angles of 0°, 45° and 60°. Experimentally measured apparent shear moduli (**A**), DNA content per dry weight (DW) (**B**), s-GAG per dry weight (**C**), Collagen per dry weight (**D**), and histology of 0° samples at 4, 8 and 12 weeks (**E**) stained for alcian blue (GAG) and picosirius red (Colagen). Scale bar = 500μm. # = $P < 0.05$ compared to unseeded scaffold (0 weeks), ## = $P < 0.05$ compared to 4 weeks, ### = $P < 0.05$ compared to 4 and 8 weeks. Results indicate mean ± SD (n = 5 per θ per time point).